Published in final edited form as:
J Geophys Res. 2000 ; 105(D16): 20663–20672. doi:10.1029/2000JD900271.

Dust resuspension without saltation

Gwen A. Loosmore and **James R. Hunt**
Department of Civil and Environmental Engineering, University of California, Berkeley, CA 94720. (loosmore@uclink4.berkeley.edu)

Abstract

Wind resuspension (or entrainment) provides a source of dust and contaminants for the atmosphere. Conventional wind erosion models parameterize dust resuspension flux with a threshold velocity or with a horizontal abrasion flux; in the absence of abrasion the models assume dust flux is transient only. Our experiments with an uncrusted, fine material at relative humidities exceeding 40% show a long-term steady dust flux in the absence of abrasion, which fits the approximate form: $F_d = 3.6 (u^*)^3$, where F_d is the dust flux (in μg/m^2 s), and u^* is the friction velocity (in m/s). These fluxes are generally too small to be significant sources of dust in most models of dust emission. However, they provide a potential route to transport contaminants into the atmosphere. In addition, dust release is substantial during the initial transient phase. Comparison with field data suggests that the particle friction Reynolds number may prove a better parameter than u^* for correlating fluxes and understanding the potential for abrasion.

1. Introduction

The resuspension of dust (crustal materials of diameter <20 μm) by wind provides a potential source of particles to the atmosphere. Many contaminants are found in or associated with dust, including metals [Hopke et al., 1980], pesticides [Risebrough et al., 1968], dioxins [Hansen and O'Keefe, 1996], and radionuclides [Anspaugh et al., 1975; Garger, 1994]. For such contaminants, small resuspension fluxes could pose important risks to human health or the environment. Resuspended dust plays a role in global climate change [Tegen et al., 1996] as well as the mediation of atmospheric chemical reactions [Dentener et al., 1996]. For these reasons, global circulation models as well as environmental risk assessment require adequate predictive models for resuspension fluxes. The dust resuspension models currently in use rely on a conceptual description of dust resuspension that is not altogether complete: These models fail to predict small, sustained fluxes that may occur below the visual threshold in the absence of abrasion. Such small fluxes are observed in the idealized experiments described in this article.

The word “resuspension” is used synonymously with “entrainment” in this article, with the connotation that particles may be continually deposited and resuspended. Mechanistically, dust may be resuspended by abrasion or through the direct action of the wind on the surface. Abrasion occurs when the surface is disturbed in some way, either mechanically, as when a vehicle drives across a field, or naturally, through saltation. Saltation is the hopping motion of sand-sized particles, which once lifted, are too large to remain suspended [Bagnold, 1954]. When the saltating particles return to the surface, the impacts can raise dust and additional saltating particles [Cahill et al., 1996; Rice et al., 1996].

For consistency among experiments, researchers characterize the velocity by the friction velocity u^* (m/s), defined as $(\tau_0/\rho)^{1/2}$, where τ_0 is the shear stress on the surface and ρ is the fluid density. Abrasive dust flux models are built on saltation models. In these models, saltation is predicted to occur only above a certain threshold friction velocity u^*_{th}, commonly taken as

the friction velocity at which movement of the sand-sized particles is first observed visually. A typical saltation model is [Gillette, 1974]

$$q=\beta u^{*2}(u^* - u^*_{th}) \quad u^*>u^*_{th}, \tag{1}$$

where q is the mass flux of saltating particles and β is a constant. The flux for $u* > u^*_{th}$ is assumed to be zero. Many similar models exist [Greeley and Iversen, 1985], dating from Bagnold's [1954] early work in this area.

An alternate mechanism for dust resuspension involves the direct removal of dust particles by the wind, in the absence of abrasion. This mechanism has been neglected in the models because saltating particles move more easily than do dust-sized particles. Adhesive forces such as van der Waals, capillarity, and cementation are orders of magnitude more important for dust particles than for sand. Moreover, owing to the nature of the boundary layer the fluid removal forces are smaller on the dust-sized particles. The wind speed available for removal scales with the log of the distance from the surface; hence dust particles experience smaller mean drag forces than do larger particles. For these reasons, visual threshold velocities reach a minimum at a diameter of ~80 μm [Chepil, 1951]: For smaller particles the effects described above increase the threshold, and above 80 μm, gravitational forces increase the threshold.

Previous experiments on aerodynamic resuspension (i.e., with no abrasive forces) have observed an initial transient dust release falling off quickly, within minutes, to neglible or zero fluxes [Bagnold, 1954; Chepil and Woodruff, 1963; Shao et al., 1993]. However, these experiments all relied on visual observation or filtration to determine the long-term fluxes, and these methods cannot properly identify small sustained fluxes. The conceptual model derived from these studies is shown schematically in Figure 1. After the transient removal, the bed is said to be stabilized with respect to that flow. This conceptual model underlies the Environmental Protection Agency (EPA) model for fugitive dust release [U.S. EPA, 1995]. The EPA model does not express the time dependence of the process but simply predicts dust mass emission for the fastest velocity above the visual threshold expected between disturbances, assuming all mass is released during the transient event and that the surface then stabilizes until disturbed again.

The research described here focuses on the effect of a steady wind on a smoothed dust bed. In contrast to the above-described models, we hypothesize that there is indeed a long-term, steady dust flux emitted from the bed, below the visual threshold, in the absence of abrasion. This flux is expected to be an increasing function of the wind speed. The remainder of this paper discusses the experiments performed and the results obtained, which support our hypothesis.

2. Experimental Methods

This experiment was designed to study nonabraded dust flux in an idealized setting so as to better understand the processes involved. The experimental conditions here are not necessarily representative of any natural Earth soil. Whereas atmospheric dust resuspension is a complex topic involving an unsteady turbulent boundary layer flowing over a changing surface in the presence of heat and moisture fluxes, this study involved a well-characterized wind tunnel flow over a smoothed bed of an idealized dust source. Ambient laboratory dust levels were maintained at a low level, and laboratory relative humidity and temperature were monitored and controlled. The ambient and resuspended dust concentrations were measured over time using TSI DustTrak light-scattering particle counters (photometers).

The wind tunnel is a modified TSI 8390 bench-top suction-type calibration wind tunnel with a test section designed specifically for these resuspension experiments (see Figure 2). The basic tunnel has two honeycombs and a coarse particle filter in the inlet. The test section is constructed of acrylic and is 2 m in length, with a square cross section of 0.1 by 0.1 m. The final 0.6 m of the test section bottom is made of a removable dish that is filled with the test soil. The area of the soil surface exposed to the wind in the tunnel is ~0.05 m × 0.5 m. The dish containing the soil was half the width of the test section to minimize wall effects. A box HEPA filter sits downwind of the soil bed and is followed by the original diffuser section. The TSI fan is controlled by a variable transformer.

Empirical relationships predict the full development of pipe flow 40 diameters downstream of the inlet [White, 1986]. The laboratory was not big enough for a four-plus meter test section, hence grade 60 silica carbide sand paper was used on the bottom surface of the test section to facilitate momentum transfer and hasten the boundary layer development. No trip wire was used, as there is evidence that these mechanisms may introduce distortions into the flow [Klebanoff and Diehl, 1952] and there was concern that these distortions might not dissipate in the short test section used here.

The tunnel velocities were measured using a TSI IFA-100 unit with cross-probe hot-film sensors. Data were collected using a National Instruments PCI E Series DAQ board with LabVIEW. The highest expected frequency of turbulent eddies in the tunnel was estimated at ~20 kHz from energy conservation principles. To prevent aliasing of these components and to best approximate simultaneous sampling for the two sensors on the cross probe, anemometer voltage signals were sampled at 100 kHz per sensor, for 2 s per run. This duration proved sufficient for generation of turbulent statistics, and the mean velocities at a point were quite clearly steady over this time period. Velocity data were measured at a central location both span and lengthwise, at intervals of 2.54 mm (0.1 inches) above the bed. Velocity profiles were also taken at two off-center locations to estimate the spanwise deviation of the velocity profile.

The idealized soil used in these experiments was Arizona Test Dust, also known as ISO-12103-1, milled to a precise particle size distribution by Powder Technology Inc. This alumino-silicate dust has an upper size limit just exceeding 10 μm and therefore serves as a standard source of PM-10. The diameter mode based on volume is 5.0 μm. Approximately 10% by volume is composed of particles smaller than 2 μm in diameter. This dust is smooth with no visible aggregates and poured easily into the test beds. The tops of the beds were smoothed as much as possible to present little or no apparent roughness to the wind in the tunnel. Beds were left to equilibrate with room air for at least 1 hour after being filled with dust before exposure to the test wind. For replicate runs, dust was added to the top of the beds and the surfaces smoothed again.

The DustTrak aerosol monitors were used to measure particle concentrations in the ambient laboratory air and up and downwind of the dust bed during experiments. These monitors measure light scattered at 90° from particles drawn into the unit. The units are calibrated for the particle size distribution of Arizona Test Dust, and with this calibration the light-scattering signal is converted to a real-time particle mass concentration. The unit can detect concentrations over the range 0.001–100 mg/m^3. When the concentration exceeds 100 mg/m^3 and when sampling at 1 Hz, the units will occasionally output negative values, indicating that the concentration in the measuring volume was so high as to obscure the photometer. Other negatives may occur owing to electrical transients in the power supply, which was avoided by using battery packs. The sensor flow rate is adjustable over a small range. The sampling frequency is also adjustable: For these experiments, measurements were recorded at a frequency of 1 Hz.

The sampling inlet and tubing were designed for isokinetic sampling and to minimize particle deposition. The nozzle was cut to a knife edge, and the nozzle diameter was chosen so that the inlet velocities possible with the DustTrak flow rate range would match the impinging velocity on the nozzle. The upwind nozzle was placed in the wind tunnel inlet on a side wall, and the downwind nozzle was placed just downwind of the soil bed. The nozzle entrances were 0.005 m from the walls. The sampling tube length and curvature were minimized as much as possible.

Experiments were performed for the range of velocities available as follows. A filled dust bed was set in the tunnel. The ambient room concentrations were measured, and DustTrak units were set in place to sample upwind and downwind of the bed. Then the fan motor was quickly brought up to the desired wind speed, which took several seconds. Concentrations were logged at 1 s intervals for at least 30 min, well beyond the duration of transient fluxes observed in previous work. After ~30 min, the upwind and downwind sampling was ceased, and the downwind unit was moved upwind to take another 5 min record, with the tunnel operating, to provide an alternate means to compute the net concentration. The zero baselines of the DustTrak units were checked before and after each experiment and adjusted if necessary.

Temperatures were monitored during experiments using an ordinary thermometer. Relative humidities were computed by use of wet- and dry-bulb temperature measured with a battery-powered psychrometer. The literature predicts no influence of relative humidity on particle adhesion at relative humidities below ~65% [Zimon, 1969]. The temperature and relative humidity for the dry experiments fell in the ranges of 17°–21°C and 40–50%, respectively. During the 30 min duration of a particular experiment, there was no measurable change in either the room temperature or relative humidity for these dry experiments, although the relative humidities could be measured reliably only within a few percent. In addition, to investigate the influence of relative humidity on these processes, the laboratory was sealed and humidified using two cool-air humidifiers and a steam humidity unit. It was extremely difficult to maintain a constant humidity above ~55%, given that the room could not be perfectly sealed. Note that the room has an approximate volume of 115 m^3; with the air flow rate through the tunnel as high as 0.22 m^3/s, almost four room volumes of air pass through the tunnel in a 30 minute experiment.

3. Computational Methods

Friction velocities were computed from the velocity profiles using several methods. The semilogarithmic regression (which relies on the dependence of U on the logarithm of y) is perhaps the most widely used in the dust entrainment literature. Barenblatt and Chorin [1998] have presented an analysis that questions the semilogarithmic profile; their power law relationship was also used in this analysis to compute u^*. In addition, the wall shear stress was inferred by extrapolating the total shear stress profiles to the wall, where the total shear stress was computed from the velocity data as

$$\tau = \rho\overline{uv} - \mu(\partial U/\partial y). \quad (2)$$

Long-term concentrations were computed by averaging over the final 10 min of the experiment, well beyond the transient peak. When necessary, the average concentrations were adjusted for zero slippage of the monitors. The rare negative values were processed out before averaging by setting them equal to the next positive value, a choice which should be conservative, as early experiments confirmed that negative values were indicative of concentrations too high to be recorded properly.

Net concentrations were computed by subtracting the long-term average upwind concentration values from the downwind values. Two upwind records were available: the simultaneous upwind sample from the resuspension run and the postexperiment ambient using the same DustTrak unit as was used for the downwind measurement. Both have some advantage: The simultaneous record is a true record of the tunnel concentrations sampled upwind during an experiment, but this was necessarily obtained using a different DustTrak monitor. Even though the zero baselines were checked frequently, because the zero slip (change in zero baseline with temperature and dust sampled) of the two units were not identical, the postrun record was also utilized. The differences between the net concentrations derived using the two different upwind values were, on average, $<1.5\ \mu g/m^3$; roughly 45% were between 1.5 and $3\ \mu g/m^3$. Net concentration values computed using the simultaneous upwind records were used for the flux calculations, presented below.

Numerical methods were necessary to estimate the resuspension flux from the time series concentration values measured at a fixed height above the bed. It was not possible to compute a mass balance to solve for the resuspension flux from the concentration measurements. The average long-term concentration measurement at one height is not equivalent to the average particle mass concentration in the tunnel: The flux from the bed will generate a concentration profile downwind, with concentrations highest nearest the bed. Because the shape of that profile is not known a priori for the wind tunnel, the point concentration measurement yields no information about the total mass flux through the tunnel. Nor was it possible to generate a profile by taking concentration data at multiple heights. The velocity increases rapidly with height above the surface, so to achieve isokinetic sampling, it was necessary to place the nozzle as close to the surface as possible. In addition, slight differences in the roughness of the bed surface could cause variations in the resuspension flux from run to run, and there was variability in replicates of the concentration measurements observed at the same fan speed. Therefore generation of profiles from concentration measurements taken at different heights for different runs would be physically questionable.

Nor was it possible to measure all of the resuspended mass leaving the bed. The bed itself weighed several kilograms, and because the total mass resuspended during an experiment was on the order of milligrams, it was impossible to accurately determine the mass lost by weighing the bed. Most importantly, even were it possible to determine the weight of all of the resuspended mass, using this value to compute a mass balance would artificially inflate the computed resuspension flux by confounding the short-term transient high dust release event with the longer-term steady flux.

In the atmosphere, researchers typically assume a model for the concentration profile and infer a flux from the concentration gradient, using the eddy viscosity as the particle diffusivity, as in the work by Nickling and Gillies [1989] described below. The uncertainties associated with that approach have not been sufficiently addressed. In order to compute a more precise resuspension flux for the present experiment, a more direct numerical approach was taken, which recognized that resuspended dust particles diffuse and advect through the test section. The vertical particle diffusivity was assumed equivalent to the turbulent eddy viscosity ν_t, which amounts to assuming that momentum and particles are dispersed analogously by the turbulent fluctuations. Thus the particle diffusivity was computed from the Reynold's stress and mean velocity from

$$D_t \approx \nu_t = \overline{uv}(\partial U/\partial y)^{-1}. \tag{3}$$

Natural cubic splines were used to interpolate the measured values of U, V, and $u\bar{v}$. The interpolated values of $U(y)$ were used to estimated the gradient $\partial U/\partial y$ using centered differences. Then D_t was computed within the boundary layer at the interpolated points. Values of $U(y)$, $V(y)$, and $D_t(y)$ were used to computationally estimate the flux from the bed, using the measured net concentrations, as follows. The system was assumed to be two-dimensional only, with neither advection nor diffusion in the z direction. The variable x represents the horizontal distance down the soil bed, and y represents the vertical distance from the bed surface. The resuspension flux F_d (in mg/m^2 s) was assumed to be constant with x. The horizontal and vertical mean velocities U and V and the turbulent diffusivity D_t were assumed to be functions of y only. The equation representing the steady state process was

$$U(y)\frac{\partial C}{\partial x}+V(y)\frac{\partial C}{\partial y} =\frac{\partial}{\partial y}\left[D_t(y)\frac{\partial C}{\partial y}\right], \tag{4}$$

which assumed negligible diffusion in the horizontal direction.

The upwind boundary condition was $C(x = 0) = 0$; that is, no mass advects in from upwind. The upper boundary condition was $C(y = H) = 0$, where H is the top of the boundary layer. The bottom boundary condition was provided by the resuspension flux F_d. No downwind boundary condition is needed for this solution method, which propagates the solution forward in space. The computational domain was set up to mimic the actual bed length and test section height, so that the downwind edge of the computational domain mapped onto the downwind bed edge for comparing computed and measured concentrations.

Conceptually, the goal was to find the flux value, the source term, that would cause the numerical simulation to yield the same concentration as the net measured value at the sampling point. This process involved assuming a resuspension flux, solving the equations, and then adjusting the flux source term and repeating until the numerically computed concentration at the sampling height matched the net measured concentration at steady state.

In the computational domain the resuspension flux from the bed was the only source of mass. By assumption, no mass returns to the cell from the next column of cells (i.e., from farther downwind in the tunnel), so the mass concentrations for a column of cells depends only on what advects in from the preceding column and on what diffuses into adjacent cells in this column. Therefore a discretized approximate mass balance may be written for each grid cell in the column of cells, generating a closed system of linear equations, where there is a source term for the bottommost cell due to the resuspension flux and the topmost concentration is assumed to be zero (an assumption that was confirmed by the calculations). The system of linear equations may be written as the matrix equation:

$$\overline{\overline{\mathbf{A}}}\mathbf{C}=\mathbf{b}, \tag{5}$$

where $\mathbf{A}$ is a tridiagonal matrix, $\mathbf{b}$ contains the upwind concentration values and the source term for the bottommost cell, and the vector $\mathbf{C}$ is the set of unknown concentrations for the given column. At the far upwind edge of the domain, no mass advects into the cells, by assumption. Thus the equations for the first column are completely specified, and the concentrations may be obtained with a tridiagonal solver. In this case, the Thomas algorithm

was used [see, e.g., Hoffman, 1992, p. 46]. The computed concentrations for the first column are then used to compute the matrix **A** for the second column, and the solution is thus propagated across the computational domain to the downwind edge.

4. Results

4.1. Velocity Characterization

Boundary layer profiles for a series of velocities are shown in Figure 3; these data show a boundary layer over a few centimeters and then a flat-profiled core flow. The average horizontal centerline velocities U_{cl} from the velocity profiles at the midpoint of the bed are presented in Table 1. The turbulent intensities took on values near 10% near the wall, falling off to a few percent above the boundary layer. Because the test section is short, some continued development of the boundary layer was expected along the test bed, but preliminary tests showed this velocity change to be less than ~5%. Measurements taken across the transverse span of the bed at the far downstream edge showed that these transverse velocities were, on average, consistent within ~5%, with some deviations as large as 12%. The friction velocities computed from the three methods are presented in Table 1: The total shear extrapolation results in values smaller than the other methods by 10–30%.

4.2. Concentration and Fluxes

Because the tunnel walls are transparent, it was possible to observe the dust beds during the experiments. No dust movement was observed during these experiments; thus all velocities were below the visual threshold velocity for movement. Nor did the beds appear disturbed after an experiment. The net concentration records show a discernable peak lasting a few minutes, followed by a fluctuating, nonzero long-term concentration. A sample concentration record is presented in Figure 4, in which the downwind 1 s concentration records (in mg/m^3) are plotted versus time. The ambient average concentration (upwind) is also shown; the raw 1 s ambient data are not presented in order to keep the graph legible. The ambient average is 0.006 mg/m^3, and the long-term average downwind concentration after 20 min is 0.012 mg/m^3. The concentration scale is logarithmic, and the initial high values corresponding to the peak resuspended mass are, evidently, at least 3 orders of magnitude higher than the long-term concentration. The peak lasts for a few minutes only, but the downwind concentration remains higher, on average, than the upwind values for the entire 30 min of the experiment.

Flux results are presented in Figure 5, using the friction velocities calculated from the semilogarithmic fit: This graph includes data for relative humidities in the low (40–50%) and medium (60–70%) range. Some variability is evident, although there is also a clear trend of increasing flux with u^*. The best fit relationship for the low relative humidity data, computed without the outlier, shows flux increasing as a function of the friction velocity cubed:

$$F_d = 3.6(u^*)^3 (\mu g/m^2 s) \quad R^2 = 0.77. \tag{6}$$

It is interesting to note that Bagnold [1954] predicted and confirmed a third-power relationship for the movement of saltating particles.

The effect of the intermediate relative humidity on the flux results is ambiguous. In the medium range of humidity, net concentrations fell in the midrange of dry measurements for all but the lowest velocities studied. At these lower velocities the humid air results were slightly elevated over the dry air values. Whether there is a statistically significant difference has not been determined.

Nonzero resuspension fluxes were observed for all velocities tested in this study. Whether this dust has a genuine (not visual) threshold friction velocity, below which truly no dust is removed, could not be determined, as 0.62 m/s was the lowest friction velocity possible in this facility.

As noted, the concentration records showed an initial peak falling within a few minutes to the steady value. The mass of dust released during the peak period is also potentially an important dust source. In order to compare this peak mass generation to the long-term flux the question was asked, How long would the long-term flux need to exist to generate as much mass per unit area as the transient peak? To answer this question, it was necessary to estimate the total mass resuspended from the entire bed during the peak period because the mass sampled by the DustTrak represents only a fraction of this total mass resuspending. Hence, to calculate the total mass generated during the peak, peaks were assumed to last 5 min, well beyond the transient resuspension observed by Shao et al.'s [1993] experiments. The masses sampled during the peak and long-term periods were computed from the concentration records and sampler flow rate. It was then assumed that the relationship between total mass resuspended and sampled mass was constant for a given wind speed. In other words, the sampled mass was assumed to always have the same relationship to the actual resuspending mass, whether in the peak or long-term records, which is equivalent to assuming that the shape of the concentration profiles are similar. This ratio of total resuspended mass M_T to sampled mass M_S was then computed from the long-term flux F_d and sampled mass $M_{s,lt}$, as

$$\frac{M_T}{M_S}=\frac{F_d A\Delta t}{M_{S,lt}}, \tag{7}$$

where A is the bed area and Δt is the time over which the sampled mass is summed. Similarly, the total mass resuspended during the 5 min peak $M_{T,p}$ could thus be estimated from the mass sampled during the peak $M_{S,p}$ as

$$M_{T,p}=(M_T/M_S)M_{S,p}, \tag{8}$$

and the time for the long-term flux to generate the same mass as the peak could then be computed from

$$T=M_{T,p}/F_d A. \tag{9}$$

These times (averaged over replicates) are presented in Table 1. There is a general downward trend with velocity: The higher the velocity, the less important the peak mass relative to the long-term flux. The reason for the very high peak release at U_{cl} = 15 m/s is not known, although only one experiment was performed at that speed. Generally, many hours would be necessary for the long-term flux to match the peak contribution, demonstrating the potential need for adequate understanding of the peak mass generation process in dust flux prediction.

5. Discussion

5.1. Flux Values

The dust fluxes observed in these experiments are small relative to values expected for abraded scenarios. Figure 6 presents these fluxes replotted as a function of particle friction Reynolds

number, $Re_p^*=du^*/\nu$, computed using a diameter of 5 μm for the Arizona Test Dust. On the same plot can be seen data from a series of field experiments performed by Nickling and Gillies [1989], where the mean soil diameter is used to generate this Reynolds number. Although the values for the current experiment scale only with u^*, the field results depend on both u^* and d. Nickling and Gillies' results were obtained in a open-bottom wind tunnel set on natural soil surfaces and potentially included abrasion of the surface. In addition, these researchers included peak masses in their flux computations: They collected suspended mass on a filter over a time period of at least 10 min, and the average concentration was computed from that mass and the flow rate and time of experiment. They assumed that the concentration follows a power law relationship with height:

$$dC/dy = -0.3(C/y). \tag{10}$$

By setting the diffusivity equal to the turbulent viscosity in a constant-stress boundary layer

$$D_t = 0.4u^* y, \tag{11}$$

an estimated flux can be obtained from a single concentration measurement [Nickling and Gillies, 1989]:

$$F_d = 0.12u^* C. \tag{12}$$

Applying this flux equation to the long-term net concentrations presented here underestimates the long-term flux relative to the numerically computed values by a factor of 3–5. To better compare the current results with Nickling and Gillies' estimated fluxes, it is necessary to include the peak mass. Thus concentrations for the current experiments were recomputed analogously to Nickling and Gillies' experiments by calculating the total net mass sampled for the first 15 min of the experiments. The long-term fluxes computed from those values are also shown in Figure 6; this method overestimates the long-term flux, relative to the numerically computed values, by an order of magnitude.

Nickling and Gillies' fluxes are greater still than even these increased values, again suggesting the presence of abrasion in their experiments; while they did not have fully developed saltation, some abrasion would generate more dust than none. Abrasion will occur only if there are particles larger than dust that move within the site of interest. The presence of larger particles thus increases the possibilities for resuspension, as would a faster wind, so it is interesting to examine the results as a function of particle friction Reynolds number. In the current experiment the diameters are low; hence Re_p^* is low, and there is no chance of abrasion. The presence of sand-sized aggregates or particles will raise the Re_p^* and grant the possibility of abrasion. Thus the parameter Re_p^* may serve as a measure of the availability of resuspension mechanisms, either by increased wind or by abrasion.

5.2. Comparison to Literature Data

An estimate of the relative magnitudes of abraded and non-abraded flux values may be obtained by comparing the experimental results here to dust flux models in the literature. Consider, for example, a model that relates dust flux linearly to the abrasive flux, with the constant of proportionality dependent on soil type, as described by Marticorena et al. [1997]. Using the

saltation model from Gillette [1974] with a constant of proportionality of 10^{-6}/cm yields the following dust flux model for steady state abrasion:

$$F_d = 10,000 u^{*2} (u^* - u^*_{th}) \ (\mu g/m^2 s), \tag{13}$$

where the pertinent threshold is for saltation to begin. For u^* much larger than the threshold this equation predicts a dust flux ~3000 times larger than the nonabraded steady fluxes presented above. Only for u^* very close to the threshold would the nonabraded flux be important, although the steady saltation model might not apply in this situation. Below the saltation threshold, however, the saltation model predicts no flux, which as the current experiments show, is incorrect. These abrasion-induced dust flux models have not been generally validated with field data, nor is it clear that these models apply for sporadic abrasion or gusty wind events. In recognition of these difficulties, researchers are developing impact-based models to relate the abrasive energy available to the dust flux [Shao et al., 1993, 1996].

Even though the nonabraded fluxes may be significantly smaller than those that develop under abrasion, there are sites at which small fluxes could pose hazards to human health and the environment. These could include wastewater sludges, radionuclide-contaminated areas, toxic spills, pesticide-sprayed areas, and the like. Evaluation of the risks associated with resuspension of these hazardous substances will require a robust model of nonabrasive resuspension fluxes, including both steady and peak mass generation. In addition, although the idealized powdery soil for these experiments may not be representative of any terrestrial situation, such conditions may be found in other environments, such as on Mars.

Because the peak mass can represent a significant fraction of the total dust resuspended in a nonabraded scenario lasting only a few hours, it will be important to understand when peaks occur. In a natural environment, peaks may occur each time the wind changes direction or magnitude. There could be a genuine threshold effect, such that peaks are suppressed below that velocity. In addition, surfaces exposed for some time to a given velocity could develop resistance to all smaller velocities, if only because all particles removable at those forces have been resuspended. The dust fluxes from direct wind resuspension will depend on the time of exposure and potentially on the exposure history. These issues have not been addressed by the models.

5.3. Comments on Medium Relative Humidity Experiments

The observation of a slight increase in net concentration for the slower velocities, for relative humidities in the range of 60–70%, may be due to a slight increase in aggregation at the bed. Aggregation could drive up the mean particle size at the surface, and the aggregates would move more readily than the isolated particles. This is strictly a conjecture and deserves additional study. As noted previously, it was difficult to maintain the humidity even at these intermediate levels. The lower moist-air flux value at $u^* = 0.62$ m/s occurred for a room relative humidity of ~60%, while the higher occurred for a relative humidity near 70%. Similarly, the high moist-air flux seen at $u^* = 0.77$ occurred for a relative humidity near 70%. All of the other moist air fluxes occurred for relative humidities below ~67%. Hence the aggregation effect may be occurring only for relative humidities >67%, which would explain why there was no apparent effect on the flux for the higher velocity runs. These relative humidity values are approximate, valid within a few percent.

6. Conclusions/Future Research Needs

The results described here support the hypothesis that a steady, long-term dust flux can occur from a smoothed dust bed under the effect of a steady wind below the visual threshold in the absence of abrasion. This dust flux scales as the third power of the friction velocity. The initial transient peak mass fluxes also generate significant dust relative to the long-term fluxes. These results confirm that the current conceptual model of dust resuspension may be inappropriate for predicting small fluxes relevant to contaminant transport scenarios. Several questions remain for future investigation.

1. There is a need for field confirmation of the long-term flux. This will require a careful experimental design to identify and compute resuspension fluxes from a local site that corrects for upwind sources. Use of one concentration value with simplifying models to predict fluxes has been shown to overestimate the flux in the present experiment. Hence it would be preferable to generate a true concentration profile or to measure the turbulent diffusivities directly and solve for the fluxes numerically, as in the present experiments.
2. The transient peak masses need additional study for prediction and for identification of the situations where transient removal will dominate.
3. The effects of moisture and heat fluxes and the changing atmospheric wind on nonabraded dust resuspension need quantification.
4. The trend of increasing flux with soil particle friction Reynolds number deserves additional study, as this parameter may better represent the potential for dust release than does the historical use of u^* in such analyses.
5. The potential for the small fluxes measured in these experiments to transport contaminants in the environment deserves further attention; in particular, there must be recognition that the visual threshold is not an appropriate parameter for dust release, and contaminants may be moving into the atmosphere by resuspension from sources that have been evaluated incorrectly using conventional models.

Acknowledgments

This research was supported by the National Institute of Environmental Health Sciences (NIH) (P42 ES04705), with partial funding for G.A.L. provided by the EPA STAR Fellowship program, and its contents are solely the responsibility of the authors and do not necessarily represent the official views of the NIEHS, NIH, or EPA. J. Shinn provided facilities at Lawrence Livermore National Laboratory. An anonymous reviewer provided the suggestion that this experiment may relate directly to conditions found on Mars.

References

Anspaugh LR, Shinn JH, Phelps PL, Kennedy NC. Resuspension and redistribution of plutonium in soils. Health Phys 1975;29:571–582. [PubMed: 1205859]

Bagnold, RA. The Physics of Blown Sand and Desert Dunes. Methuen; New York: 1954. p. 265

Barenblatt GI, Chorin AJ. Turbulence: An old challenge and new perspectives. Meccanica 1998;33:445–468.

Cahill TA, Gill TE, Reid JS, Gearhart EA, Gillette DA. Saltating particles, playa crusts, and dust aerosols at Owens (Dry) Lake, California. Earth Surf Processes Landforms 1996;21:621–639.

Chepil WS. Properties of soil which influence wind erosion, IV, State of dry aggregate structure. Soil Science 1951;72:387–401.

Chepil WS, Woodruff NP. The physics of wind erosion and its control. Adv Agron 1963;15:211–302.

Dentener FJ, Carmichael GR, Zhang Y, Lelieveld J, Crutzen PJ. Role of mineral aerosol as a reactive surface in the global troposphere. J Geophys Res 1996;101(D17):22,869–22,889.

Garger EK. Air concentrations of radionuclides in the vicinity of Chernobyl and the effects of resuspension. J Aerosol Sci 1994;25(5):745–753.

Gillette DA. On the production of soil wind erosion aerosols having the potential for long range transport. Atmos Res 1974;8:735–744.

Greeley, R.; Iversen, JD. Wind as a Geological Process on Earth, Mars, Venus, and Titan. Cambridge Univ Press; New York: 1985. p. 333

Hansen LG, O'Keefe PW. Polychlorinated dibenzofurans and dibenzo-p-dioxins in subsurface soil, superficial dust, and air extracts from a contaminated landfill. Arch Environ Contam Toxicol 1996;31:271–276. [PubMed: 8785012]

Hoffman, JD. Numerical Methods for Engineers and Scientists. McGraw-Hill; New York: 1992. p. 825

Hopke PK, Lamb RE, Natusch DFS. Multielemental characterization of urban roadway dust. Environ Sci Technol 1980;14(2):164–172.

Klebanoff, PS.; Diehl, ZW. Natl Adv Comm for Aeronaut. Washington, D. C.: 1952. Some features of artificially thickened fully developed turbulent boundary layers with zero pressure gradient; p. 1165-1191.

Marticorena B, Bergametti G, Aumont B, Callot Y, N'Doumé C, Legrand M. Modeling the atmospheric dust cycle, 2, Simulation of Saharan dust sources. J Geophys Res 1997;102(D4):4387–4404.

Nickling, WG.; Gillies, JA. Emission of fine-grained particulates from desert soils, in. In: Leinen, M.; Sarnthein, M., editors. Paleoclimatology and Paleometeorology: Modern and Past Patterns of Global Atmospheric Transport. Kluwer Acad.; Norwell, Mass.: 1989. p. 133-165.

Rice MA, Willetts BB, McEwan IK. Wind erosion of crusted soil sediments. Earth Surf Processes Landforms 1996;21:279–293.

Risebrough RW, Huggett RJ, Griffin JJ, Goldberg ED. Pesticides: Transatlantic movements in the northeast trades. Science 1968;159:1233–1236. [PubMed: 5711757]

Shao Y, Raupach MR, Findlater PA. Effect of saltation bombardment on the entrainment of dust by wind. J Geophys Res 1993;98(D7):12,719–12,726.

Shao Y, Raupach MR, Leys JF. A model for predicting aeolian sand drift and dust entrainment on scales from paddock to region. Aust J Soil Res 1996;34:309–342.

Tegen I, Lacis AA, Fung I. The influence on climate forcing of mineral aerosols from disturbed soils. Nature 1996;380:419–422.

United States Environmental Protection Agency (U.S. EPA). AP-42: Compilation of Air Pollutant Emission Factors, vol 1, Stationary Point and Area Sources. 5th. Off. of Air Quality Planning and Standards; Research Triangle Park, North Carolina: 1995.

White, FM. Fluid Mechanics. McGraw-Hill; New York: 1986. p. 732

Zimon, AD. The Adhesion of Dust and Powder. Plenum; New York: 1969. p. 424

Notation

C	dust concentration, mg/m^3.
d	particle diameter, m.
D	Hydraulic diameter, m.
D_t	turbulent diffusivity, m^2/s.
F_d	dust flux, mg/m^2 s or μg/m^2 s.
H	top of the boundary layer, m.
q	mass flux of saltating particles or horizontal flux, g/ms.
Re	pipe Reynolds number, equal to UD/ν.
Re_p^*	particle friction Reynolds number, equal to u^*d_p/ν.
U	mean horizontal velocity, m/s.

U_{cl}	mean horizontal centerline velocity, m/s.
u	fluctuating component of horizontal velocity, m/s.
v	fluctuating component of vertical velocity, m/s.
$u*$	friction velocity, equal to $\sqrt{\tau_0/\rho}$, m/s.
u^*_{th}	threshold friction velocity, m/s.
β	constant.
ν	fluid kinematic viscosity, m^2/s.
ν_t	turbulent viscosity, m^2/s.
ρ	air density, kg/m^3.
τ	shear stress or momentum flux, kg/m s^2.
τ_0	shear stress on wall, kg/m s^2
τ_t	turbulent shear stress, kg/m s^2

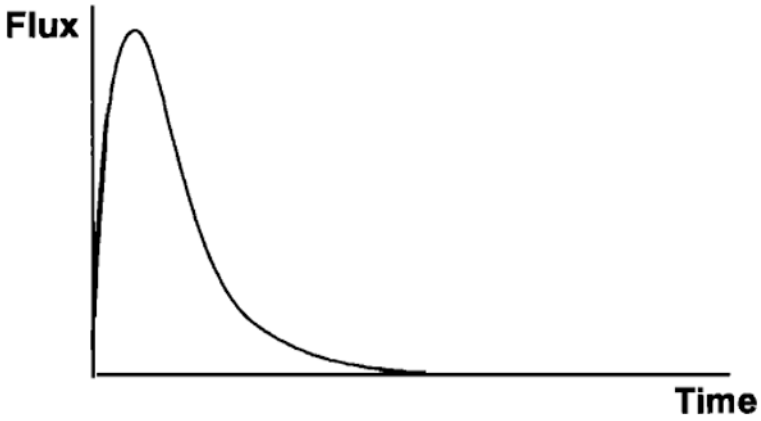

Figure 1.
The conceptual trend of nonabraded dust resuspension over time.

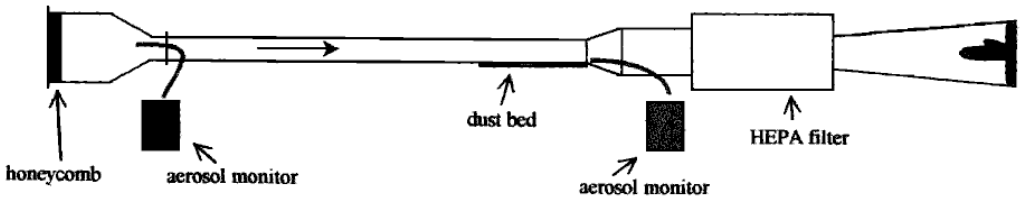

Figure 2.
Modified wind tunnel for dust resuspension study.

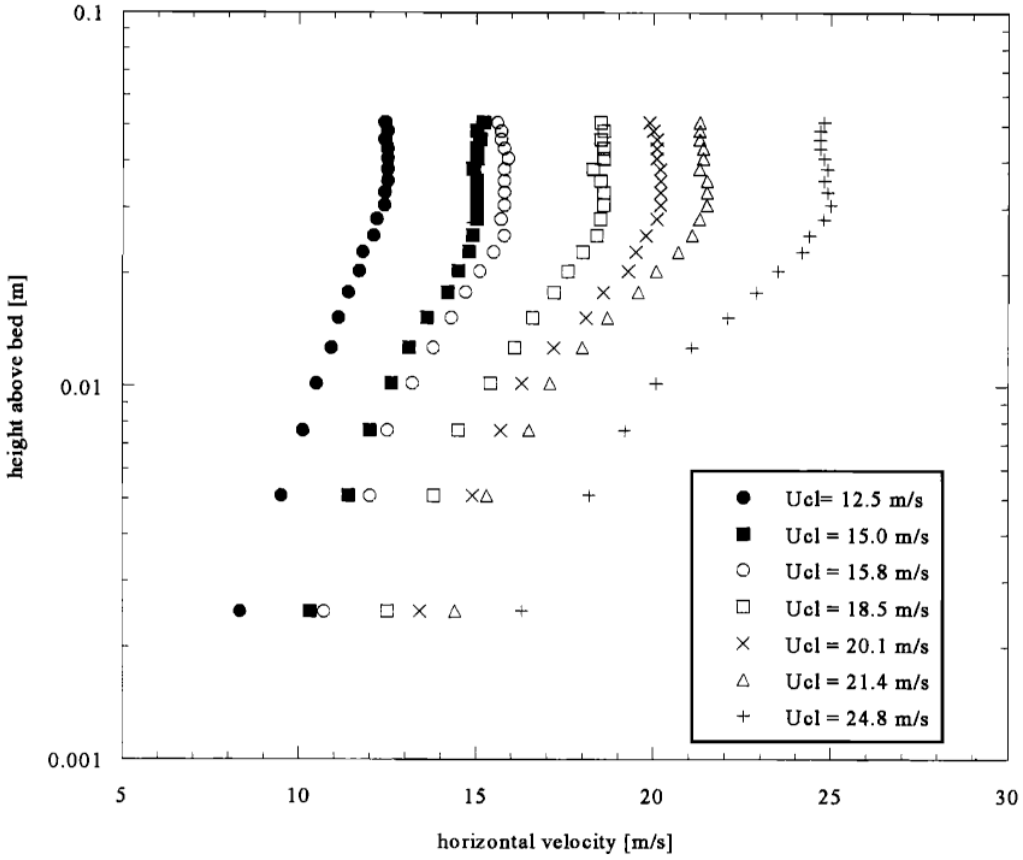

Figure 3.
Velocity profiles for various centerline velocities U_{cl}.

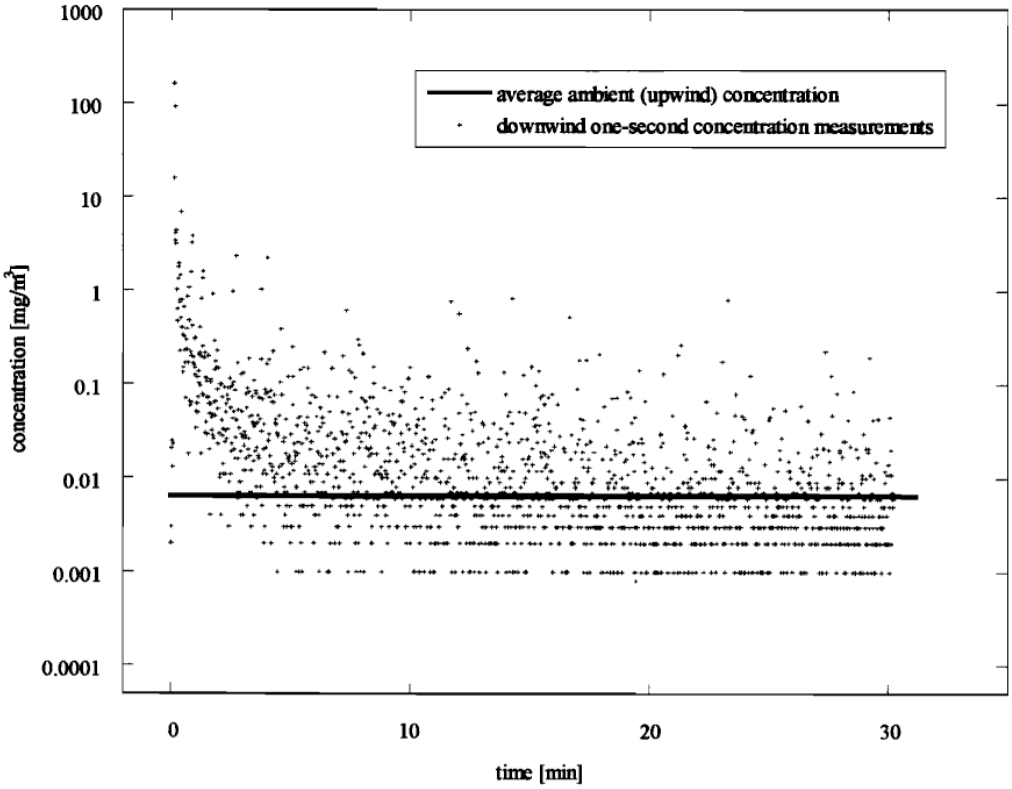

Figure 4.
A sample raw concentration record for u^* = 1.0 m/s.

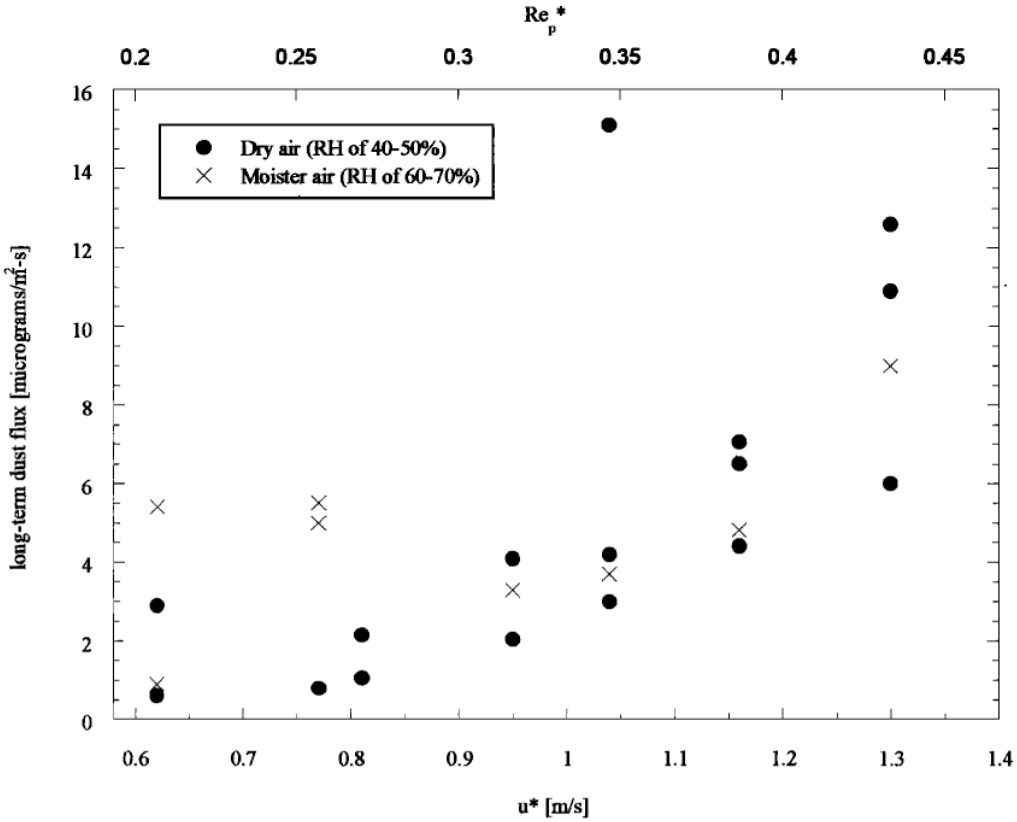

Figure 5.
Long-term dust flux results.

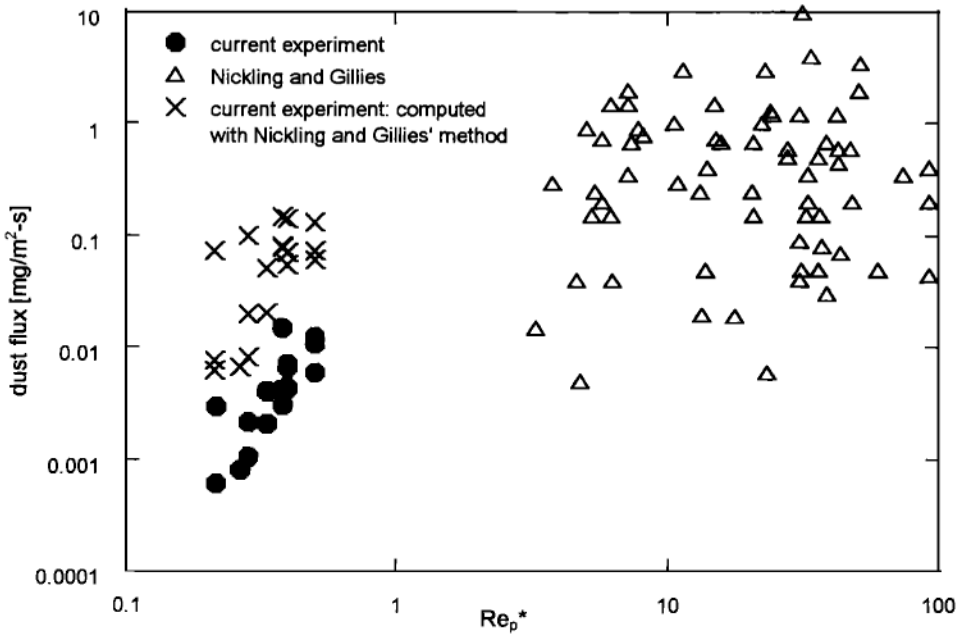

Figure 6.
Current results plotted against data from Nickling and Gillies [1989] showing dependence on particle friction Reynolds number and flux method.

Table 1

A Summary of the Experimental Results: Velocity and Dry-Air Flux and Concentration Data Averaged Over Replicates

	u^*, m/s							
U_{cl}, m/s	Semilog Fit to 1.8 cm	Power Law	From Total Shear	Number of Replicates for Dry-Air Runs	Peak Mass (5 min), mg	Steady State Concentration, $\mu g/m^3$	F_d, $\mu g/m^2$ s	Hours for F_d to Match Peak Mass
12.5	0.62	0.64	0.58	3	3.0	7	2	26
15.0	0.77	0.79	0.60	1	8.0	2	1	110
15.8	0.81	0.83	0.70	3	3.0	5	2	18
18.5	0.95	0.98	0.76	2	3.5	8	3	18
20.1	1.0	1.0	0.87	3	10.1	16	8	16
21.4	1.2	1.1	0.95	3	8.8	11	6	16
25.8	1.3	1.3	1.1	3	6.0	18	10	9